Marangoni boundary layer flow and heat transfer of copper-water nanofluid over a porous medium disk

Cite as: AIP Advances **5**, 107225 (2015); https://doi.org/10.1063/1.4934932
Submitted: 18 September 2015 • Accepted: 12 October 2015 • Published Online: 27 October 2015

Yanhai Lin and Liancun Zheng

AIP ADVANCES **5**, 107225 (2015)

Marangoni boundary layer flow and heat transfer of copper-water nanofluid over a porous medium disk

Yanhai Lin[1,a] and Liancun Zheng[2]
[1]*School of Mathematical Sciences, Huaqiao University, Quanzhou 362021, P.R. China*
[2]*School of Mathematics and Physics, University of Science and Technology Beijing, Beijing 10083, P.R. China*

(Received 18 September 2015; accepted 12 October 2015; published online 27 October 2015)

In this paper we present a study of the Marangoni boundary layer flow and heat transfer of copper-water nanofluid over a porous medium disk. It is assumed that the base fluid water and the nanoparticles copper are in thermal equilibrium and that no slippage occurs between them. The governing partial differential equations are transformed into a set of ordinary differential equations by generalized Kármán transformation. The corresponding nonlinear two-point boundary value problem is solved by the Homotopy analysis method and the shooting method. The effects of the solid volume fraction, the permeability parameter and the Marangoni parameter on the velocity and temperature fields are presented graphically and analyzed in detail. [http://dx.doi.org/10.1063/1.4934932]

I. INTRODUCTION

Nanofluids, defined as suspended nanoparticles with the size of 1 to 100 nm inside fluids, have drawn vast attention due to recently claimed high performance in heat transfer in the literature.[1] Studies have shown that adding nanoparticles (copper, silver, iron, alumina, CuO, SiC, carbon nanotube, *etc.*) to base fluids (water, ethylene glycol, engine oil, acetone, *etc.*) can effectively improve the thermal conductivity of the base fluids and enhance heat transfer performance of the liquids. In recent years, the studies of boundary layer flow and heat mass transfer in porous medium with nanofluids have attracted considerable attention in many industrial, engineering, geothermal and technological fields because of its wide applications, such as polymer solutions and melts, microgravity science and space processing, petroleum industry, rotating machineries like nuclear reactors, thin polymer films flow, *etc*. Mahdi et al.[2] presented an overview of the published articles in respect to porosity, permeability, inertia coefficient and effective thermal conductivity for porous media, also on the thermophysical properties of nanofluids and the studies on convection heat transfer and fluid flow in porous media with nanofluids. Afterward, Pop and coworkers[3–5] examined magnetic field or convective boundary condition effects on mixed convection boundary layer flow and heat transfer over a flat plate embedded in a porous medium filled with nanofluids. Furthermore, Pop and coworkers[6,7] considered the Buongiorno-Darcy model to describe the flow of nanofluids saturated in porous media. Hady et al.[8] investigated effect of heat generation or absorption on the natural convection boundary-layer flow over a downward pointing vertical cone in porous medium with a non-Newtonian nanofluid. Recently, Rashad et al.[9] presented the steady mixed convection boundary layer flow past a horizontal circular cylinder in a stream flowing vertically upwards embedded in porous medium filled with a nanofluid taking into account the thermal convective boundary condition. Then, Zheng et al.[10] had a discussion on the flow and radiation heat transfer of a nanofluid over a stretching sheet with velocity slip and temperature jump in porous medium. Lately, Abbasi et al.[11]

[a]Corresponding author, E-mail: linyanhai999@hqu.edu.cn (Y. Lin) Tel: +86 0551 2269 3514 Fax: +86 0551 2269 3514

examined the Peristaltic flow of copper-water through a porous medium using the two phase flow model.

Marangoni convection flow induced by the surface tension appears in many practical projects such as crystal growth melts, spreading of thin films, nucleation vapor bubbles, semiconductor processing, welding, materials science, *etc*. For example, Arafune and Hirata[12] developed the rectangular double-crucible system to study the velocity feature of surface tension driven flow caused by temperature differences (thermal Marangoni convection) and concentration differences (solutal Marangoni convection) in In-Ga-Sb melt. Experiments showed that the typical surface velocity of solutal Marangoni convection is about 3-5 times higher than that of thermal Marangoni convection, and the results of both thermal and solutal convection could be discussed using dimensionless Reynolds, Marangoni and Prandtl numbers. Cazabat et al.[13] studied the dynamics of spreading of thin films driven by temperature gradients. It showed that the Marangoni film is formed by applying a thermal gradient along the direction of the flow and the temperature variation of the surface tension is fairly constant for many fluids far from the critical point, and therefore a constant temperature gradient creates a constant Marangoni surface stress. In addition, the surface tension gradient causes the interface current. Marangoni convection also occurs around vapor bubbles during nucleation and the growth of vapor bubbles due to the surface tension variations caused by temperature and/or concentration variations along the bubble surface.[14,15]

The basic mechanism of the Marangoni convection has been extensively investigated. Pearson[16] created the initial model and criterion of the flow mechanism induced by the surface tension. It showed that the surface tension, in most fluids at most temperatures, is a monotone decreasing function of temperature and in the case of two constituents, a function of relative concentration. Mcconaghy and Finlayson[17] studied surface tension driven oscillatory instability in a rotating fluid layer. Based on the thin film equation derived from the basic hydrodynamic equations, Bestehorn et al.[18] presented 3D large scale surface deformations of a liquid film unstable due to the Marangoni effect caused by external heating on a smooth and solid substrate. Then, Thiele and Knobloch[19] considered the behavior of thin liquid film on a uniformly heated substrate by the weakly nonlinear theory. They pointed out that once Marangoni effects are included, the resulting film is unstable. In general, the surface was assumed to vary linearly with the temperature in Marangoni boundary layer problem.[14,15,20] Further, the surface also was assumed to vary linearly with the concentration and the thermosolutal surface tension radio parameter was introduced to describe the mass transfer.[21–25] Zheng et al.[20] established the Marangoni convection over a liquid-vapor surface due to an imposed temperature gradient by the Adomian analytical decomposition technique and the Páde approximant technique. Chamkha and coworkers [21–23] considered the steady laminar MHD thermosolutal Marangoni convection in the presence of a uniform applied magnetic field in the boundary layer approximation. And exact analytical solutions for the velocity, temperature and concentration boundary layers were reported. Later on, Zhang and Zheng[24] studied MHD thermosolutal Marangoni convection with the heat generation and a first-order chemical reaction by a new method – double parameters transformation perturbation expansion method. Similarly, Zhang and Zheng[25] investigated similarity solutions of Marangoni convection boundary layer flow with gravity and external pressure. Chen[26] explored the influence of Marangoni convection on the flow and heat transfer characteristics of a power-law liquid within a thin film over an unsteady stretching surface by a standard finite difference technique based on central differences. Saravanan and Sivakumar[27] considered exactly the appearance of Marangoni convective instability in a binary fluid layer in the presence of though flow and Soret effect for both conducting and insulating bottom boundaries. Saleem et al.[28] examined entropy generation in Marangoni convection flow of heated fluid in an open ended cavity. Zheng, Lin and coworkers[29–31] investigated Marangoni convection flow and heat transfer of power law fluids or nanofluids driven by the surface temperature gradient with variable thermal conductivity. Then, Mahdy and Ahmed[32] studied the Soret and Dufour effects on the mechanical and thermal properties of steady MHD thermosolutal Marangoni boundary layer past a vertical flat. Jiao et al.[33] presented the magnetohydrodynamic (MHD) thermosolutal Marangoni convection heat and mass transfer of power-law fluids driven by a power law temperature and a power law concentration. Hayat et al.[34] considered Marangoni mixed convection flow with Joule heating and nonlinear radiation.

Motivated by the above mentioned works,[20–34] in this paper we have a study on Marangoni boundary layer flow and heat transfer of copper-water nanofluid over a porous medium disk. The temperature of the disk (the surface temperature of Cu-water nanofluid) is a quadratic function of the radius. The cylindrical polar coordinate system of the boundary layer flow and heat transfer[35,36] is established to solve the Marangoni convection problem. The governing partial differential equations are transformed into a set of ordinary differential equations by generalized Kármán transformation[35] and the solutions are presented analytically and numerically.

II. PHYSICAL MODEL AND MATHEMATIC EQUATIONS

Consider the steady, two-dimensional, laminar, boundary layer flow of a viscous, copper-water (Cu-water) nanofluid over a porous medium infinite disk in the presence of surface tension due to temperature gradient at the surface. The Cu-water nanofluid is assumed incompressible and the flow is assumed to be axisymmetric. Thermophysical properties of Cu-water nanofluid are given in Table I.[31] It is also assumed that the base fluid water and the nanoparticle Cu are in thermal equilibrium and no slippage occurs between then. No-slid and impermeability exist on the disk. The cylindrical polar coordinate system and physical model are shown in Fig. 1. Unlike the Boussinesq effect on the body force term in buoyancy-induced flow, the Marangoni surface tension effect acts as a boundary condition on the governing equations of the flow field.[21–23,29–31] The governing equations for this study are based on the balance laws of mass, momentum and energy species. Taking the above assumptions into consideration, the boundary layer governing equations can be written in dimensional form as:[35,36]

$$\frac{\partial u}{\partial r} + \frac{u}{r} + \frac{\partial w}{\partial z} = 0, \tag{1}$$

$$u\frac{\partial u}{\partial r} + w\frac{\partial u}{\partial z} = \frac{\mu_{nf}}{\rho_{nf}}\frac{\partial^2 u}{\partial z^2} - \frac{\mu_{nf}}{\rho_{nf}}\frac{u}{k}, \tag{2}$$

$$u\frac{\partial T}{\partial r} + v\frac{\partial T}{\partial z} = \alpha_{nf}\frac{\partial^2 T}{\partial z^2}, \tag{3}$$

The boundary conditions of this problem are given by:

$$\mu_{nf}\frac{\partial u}{\partial z}|_{z=0} = \frac{\partial \sigma}{\partial r}|_{z=0}, w|_{z=0} = 0, T|_{z=0} = T_0 = T_\infty + T_{const}r^2, \tag{4}$$

$$u|_{z\to\infty} = 0, T|_{z\to\infty} = T_\infty. \tag{5}$$

where, u and w are the velocity components along the r and z directions, respectively. γ_f is the kinematic viscosity of water, and k is the permeability of the porous medium. μ_{nf} is the viscosity of nanofluid, ρ_{nf} is the density of nanofluid and α_{nf} is the thermal diffusivity of nanofluid. In addition, T is the temperature of nanofluid, T_{const} is a constant, T_∞ is the temperature of nanofluid out of the boundary layer and it is a const, T_0 is the temperature of nanofluid on the disk and it is a quadratic function of r. $\tau = \mu_{nf}\frac{\partial u}{\partial z}$ is the shear stress, σ is the surface tension. Further, it is assumed that the surface tension is linear with the temperature such that:[14,15,20,29–31]

$$\sigma = \sigma_0 - \gamma_T(T - T_\infty), \quad \gamma_T = -\frac{\partial \sigma}{\partial T}|_{T=T_\infty}. \tag{6}$$

TABLE I. Thermophysical properties of Cu-water nanofluid.

	C_p (J/KgK)	ρ (kg/m^3)	k (W/mK)
Cu	385	8933	400
water	4179	997.1	0.613

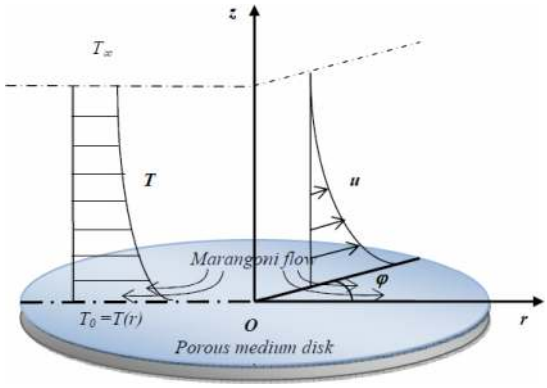

FIG. 1. Schematic of the physical system.

where σ_0 and γ_T are positive constant. The interfacial surface tension gradient which is caused by the temperature gradient at the interface induced flow as: $\partial\sigma/\partial r = \partial\sigma/\partial T \cdot \partial T/\partial r$.

Further, μ_{nf} is approximated as viscosity of the base fluid water μ_f containing dilute suspension of fine spherical particles and is given by Brinkman:[37]

$$\mu_{nf} = \mu_f(1-\phi)^{-2.5}, \tag{7}$$

The other parameters are given by:[31]

$$\rho_{nf} = (1-\phi)\rho_f + \phi\rho_s, \tag{8}$$

$$(\rho C_p)_{nf} = (1-\phi)(\rho C_p)_f + \phi(\rho C_p)_s, \tag{9}$$

$$\alpha_{nf} = k_{nf}/(\rho C_p)_{nf}, \tag{10}$$

$$\frac{k_{nf}}{k_f} = \frac{(k_s+2k_f)-2\phi(k_f-k_s)}{(k_s+2k_f)+\phi(k_f-k_s)}. \tag{11}$$

where ϕ is the solid volume fraction of the nanofluid, ρ_s is the density of the nanoparticle (Cu), ρ_f is the density of the base fluid (water). $(\rho C_p)_{nf}$ is the heat capacity of the nanofluid, $(\rho C_p)_f$ is the heat capacity of the base fluid and $(\rho C_p)_s$ is the heat capacity of the nanoparticle. k_{nf} is the thermal conductivity of the nanofluid, k_f is the thermal conductivity of the base fluid and k_s is the thermal conductivity of the nanoparticle.

III. SIMILARITY TRANSFORMATION

The following generalized dimensionless Kármán similarity variable defined as:[33]

$$\xi = z\sqrt{\Omega/\gamma_f}, \quad u = r\Omega F(\xi), \quad w = \sqrt{\Omega\gamma_f}H(\xi), \quad T = T_\infty + Ar^2\theta(\xi), \tag{12}$$

$$P = \frac{\gamma_f}{k\Omega}, \quad \mathrm{Pr} = \frac{\gamma_f(\rho C_p)_f}{k_f} = \frac{\gamma_f}{\alpha_f}, \quad Ma = \frac{T_{const}}{\Omega\mu_f}\sqrt{\frac{\gamma_f}{\Omega}}, \tag{13}$$

$$A = [(1-\phi)+\phi\frac{\rho_s}{\rho_f}](1-\phi)^{2.5}, \tag{14a}$$

$$B = [(1-\phi)+\phi\frac{(\rho C_p)_s}{(\rho C_p)_f}]\frac{(k_s/k_f+2)+\phi(1-k_s/k_f)}{(k_s/k_f+2)-2\phi(1-k_s/k_f)}, \tag{14b}$$

$$C = (1-\phi)^{2.5}. \tag{14c}$$

where Ω is a unit $[s^{-1}]$, P is the permeability parameter, Pr is the Prandtl number of the base fluid (water Pr = 7.0) and Ma is the Marangoni parameter. The governing equations (1)-(3) and the

boundary layer conditions (4)-(5) can be written as:

$$2F(\xi) + H'(\xi) = 0, \tag{15}$$

$$F''(\xi) - PF(\xi) + A[F(\xi)^2 + F'(\xi)H(\xi)] = 0, \tag{16}$$

$$\theta''(\xi) - B\,\mathrm{Pr}[2F(\xi)\theta(\xi) + H(\xi)\theta'(\xi)] = 0, \tag{17}$$

$$F'(\xi)|_{\xi=0} = -2MaC, \quad H(\xi)|_{\xi=0} = 0, \quad F(\xi)|_{\xi\to\infty} = 0, \tag{18}$$

$$\theta(\xi)|_{\xi=0} = 1, \quad \theta(\xi)|_{\xi\to\infty} = 0. \tag{19}$$

where $F(\xi)$ is dimensionless velocity, $\tau(\xi) = -\frac{1}{2C}F'(\xi)$ is dimensionless shear stress (It should be noted that $\tau = \mu_{nf}\frac{\partial u}{\partial z} = \frac{1}{C}\Omega r\mu_f\sqrt{\frac{\Omega}{\gamma_f}}F'(\xi)$, $\tau(\xi)|_{\xi=0} = -Ma$.) and $\theta(\xi)$ is dimensionless temperature.

IV. HOMOTOPY ANALYSIS SOLUTIONS

In this section, the nonlinear governing equations (15)-(17) and boundary conditions (18)-(19) are solved by HAM.[38,39] The functions $H(\xi)$ (Note: $2F(\xi) + H'(\xi) = 0$) and $\theta(\xi)$ can be expressed by the set of base functions:

$$\{\xi^i \exp(-m\xi)|i \geq 0, m \geq 0\} \tag{20}$$

in the forms

$$H(\xi) = \sum_{i=0}^{\infty}\sum_{m=0}^{\infty} a_{m,i}\xi^i \exp(-m\xi), \tag{21}$$

$$\theta(\xi) = \sum_{i=0}^{\infty}\sum_{m=0}^{\infty} b_{m,i}\xi^i \exp(-m\xi). \tag{22}$$

where $a_{m,i}$ and $b_{m,i}$ are constant coefficients. According to the rule of solution expression denoted by Liao and the boundary conditions, it is natural to choose:

$$H_0(\xi) = -2CMa + 2CMa\exp(-\xi), \tag{23}$$

$$\theta_0(\xi) = \exp(-\xi), \tag{24}$$

as the initial guesses of the functions $H(\xi)$ and $\theta(\xi)$. The auxiliary linear operators are selected as:

$$L_H = \frac{\partial^3 H}{\partial\xi^3} - \frac{\partial H}{\partial\xi}, \quad L_\theta = \frac{\partial^2\theta}{\partial\xi^2} - \frac{\partial\theta}{\partial\xi}, \tag{25}$$

Satisfying the following properties:

$$L_H[C_1 + C_2\exp(-\xi) + C_3\exp(\xi)] = 0, \quad L_\theta[C_4 + C_5\exp(\xi)] = 0. \tag{26}$$

where C_l $(l = 1,\ldots,5)$ are the arbitrary constants. If $q \in [0,1]$ and h_H, h_θ indicate the embedding and nonzero auxiliary parameters, then the 0^{th}-order deformation problems are of the following form

$$(1-q)L_H[\Phi(\xi,q) - H_0(\xi)] = qh_H H_H(\xi)N_H[\Phi(\xi,q),\Theta(\xi,q)], \tag{27}$$

$$(1-q)L_\theta[\Theta(\xi,q) - \theta_0(\xi)] = qh_\theta H_\theta(\xi)N_\theta[\Phi(\xi,q),\Theta(\xi,q)], \tag{28}$$

Subject to the boundary conditions

$$\Phi(0,q) = 0, \quad \frac{\partial^2\Phi(\xi,q)}{\partial\xi^2}|_{\xi=0} = CMa, \quad \frac{\partial\Phi(\xi,q)}{\partial q}|_{\xi\to\infty} = 0, \tag{29}$$

$$\Theta(0,q) = 1, \quad \Theta(\xi,q)|_{\xi\to\infty} = 0. \tag{30}$$

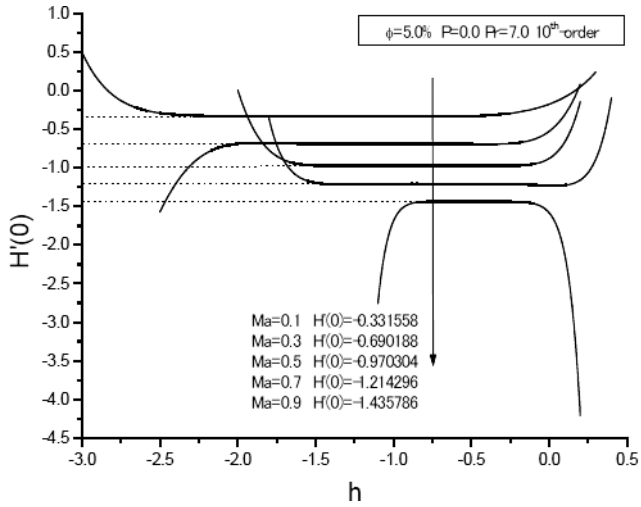

FIG. 2. The h–curves of $H'(0)$ for the 10^{th}-order approximation.

where

$$N_H = \frac{\partial^3\Phi(\xi,q)}{\partial\xi^3} + \frac{A}{2}[\frac{\partial\Phi(\xi,q)}{\partial\xi}\frac{\partial\Phi(\xi,q)}{\partial\xi} - \Phi(\xi,q)\frac{\partial^2\Phi(\xi,q)}{\partial\xi^2} - P\frac{\partial\Phi(\xi,q)}{\partial\xi}], \tag{31}$$

$$N_\theta = \frac{\partial^2\Theta(\xi,q)}{\partial\xi^2} + B\,\mathrm{Pr}[\frac{\partial\Phi(\xi,q)}{\partial\xi}\Theta(\xi,q) - \Phi(\xi,q)\frac{\partial\Theta(\xi,q)}{\partial\xi}], \tag{32}$$

where h_H, h_θ is chosen properly in such a way that these series are convergent at $q = 1$. Therefore, we have through equations are solutions series

$$H(\xi) = H_0(\xi) + \sum_{m=1}^{\infty} H_m(\xi)q^m, \quad \theta(\xi) = \theta_0(\xi) + \sum_{m=1}^{\infty} \theta_m(\xi)q^m, \tag{33}$$

in which

$$H_m(\xi) = \frac{1}{m!}\frac{\partial^m\Phi(\xi,q)}{\partial q^m}|_{q=0}, \quad \theta_m(\xi) = \frac{1}{m!}\frac{\partial^m\Theta(\xi,q)}{\partial q^m}|_{q=0}. \tag{34}$$

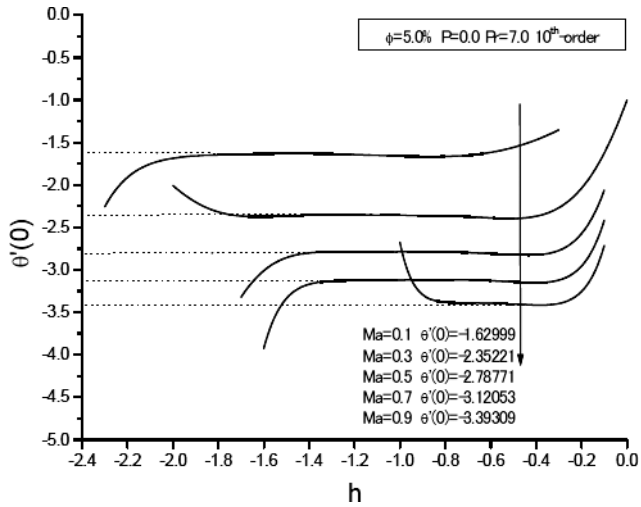

FIG. 3. The h–curves of $\theta'(0)$ for the 10^{th}-order approximation.

TABLE II. Comparison of values of $F(0)$, $H(\infty)$ and $\theta'(0)$ for different values of the solid volume fraction when $P = 0.0$, $Ma = 0.2$ and $\Pr = 7.0$.

	$F(0)$		$H(\infty)$		$\theta'(0)$	
ϕ	HAM	Numerical	HAM	Numerical	HAM	Numerical
0.0%	0.307593	0.3073370	-0.835982	-0.8316574	-2.42527	-2.428746
1.5%	0.292523	0.2922949	-0.785369	-0.7813209	-2.30518	-2.303730
3.0%	0.279196	0.2789964	-0.743459	-0.7397496	-2.19574	-2.190098
4.5%	0.267258	0.2670791	-0.708301	-0.7048761	-2.09460	-2.085970

TABLE III. Comparison of values of $F(0)$, $H(\infty)$ and $\theta'(0)$ for different values of the permeability parameter when $\phi = 5.0\%$, $Ma = 0.4$ and $\Pr = 7.0$.

	$F(0)$		$H(\infty)$		$\theta'(0)$	
P	HAM	Numerical	HAM	Numerical	HAM	Numerical
0.0	0.418092	0.4180872	-0.876228	-0.8761853	-2.58911	-2.585104
0.2	0.375794	0.3757938	-0.733096	-0.7330574	-2.42692	-2.417631
0.4	0.341499	0.3414991	-0.619493	-0.6194746	-2.27837	-2.271026
0.6	0.313600	0.3136003	-0.530582	-0.5305725	-2.14587	-2.142935
0.8	0.290670	0.2906664	-0.460763	-0.4607524	-2.03045	-2.030408

TABLE IV. Comparison of values of $F(0)$, $H(\infty)$ and $\theta'(0)$ for different values of the Marangoni parameter when $\phi = 5.0\%$, $P = 0.0$ and $\Pr = 7.0$.

	$F(0)$		$H(\infty)$		$\theta'(0)$	
M	HAM	Numerical	HAM	Numerical	HAM	Numerical
0.1	0.165779	0.1658662	-0.547885	-0.5480955	-1.62999	-1.630141
0.3	0.345094	0.3451200	-0.795323	-0.7958117	-2.35221	-2.349408
0.5	0.485152	0.4851480	-0.944018	-0.9439106	-2.78771	-2.784022
0.7	0.607148	0.6071480	-1.05609	-1.056096	-3.12053	-3.113166
0.9	0.717893	0.7178895	-1.14839	-1.148377	-3.39309	-3.384038

Differentiating m times the 0^{th}-order deformation equations (27)-(28) about q, then setting $q = 0$, and finally dividing by $m!$, we have the m^{th}-order deformation equations

$$L_H[H_m(\xi) - \chi_m H_{m-1}(\eta)] = h_H H_H(\xi) R_m^H(\xi), \tag{35}$$

$$L_\theta[\theta_m(\xi) - \chi_m \theta_{m-1}(\eta)] = h_\theta H_\theta(\xi) R_m^\theta(\xi), \tag{36}$$

with the following boundary conditions

$$H_m(0) = H_m''(0) = H_m'(\infty) = \theta_m(0) = \theta_m(\infty) = 0, \tag{37}$$

where

$$R_m^H(\xi) = H_{m-1}'''(\xi) + \frac{A}{2}[\sum_{l=0}^{m-1} H_l'(\xi) H_{m-1-l}'(\xi) - \sum_{l=0}^{m-1} H_l(\xi) H_{m-1-l}''(\xi) - P H_{m-1}'], \tag{38}$$

$$R_m^\theta(\xi) = \theta_{m-1}''(\xi) + B\Pr[\sum_{l=0}^{m-1} H_l'(\xi)\theta_{m-1-l}(\xi) - \sum_{l=0}^{m-1} H_l(\xi)\theta_{m-1-l}'(\xi)], \tag{39}$$

$$\chi_m = \begin{cases} 0, & m = 1 \\ 1, & m \geq 2 \end{cases}, \tag{40}$$

Based on the initial guesses and the auxiliary linear operators, we set: $H_H(\xi) = H_\theta(\xi) = \exp(-\xi)$. We obtain:

$$H_1(\xi) = \frac{1}{3}hCMa[-ACMa\exp(-2\xi) + (6PA + 3PA\xi + 8ACMa + 6ACMa\xi - 6 - 3\xi)\exp(-\xi) - (6PA + 9ACMa - 6)], \quad (41)$$

$$\theta_1(\xi) = \frac{1}{3}h[(-14BCMa + 1)\exp(-2\xi) - (-14BCMa + 1)\exp(-\xi)]. \quad (42)$$

In this way, the equations (35)-(37) can be solved by using Mathematica one after the other in the order $m = 2, 3, \ldots$ (See Appendix A. Supplementary material).

V. NUMERICAL SOLUTIONS

The equations (15)-(17) and the corresponding boundary conditions (18)-(19) are solved by the shooting method coupled with the Runge-Kutta scheme and the Newton method. The equations (15)-(16) and (18) are written as a system of three first-order equations in terms of the three variables y_n $(n = 1, 2, 3)$. Denoting $H(\xi)$, $H'(\xi)$ and $H''(\xi)$ by using variables y_1, y_2 and y_3 yields

$$\begin{cases} y_1' = y_2 \\ y_2' = y_3 \\ y_3' = Py_2 + A(y_1y_3 - 0.5{y_2}^2) \end{cases}, \quad (43)$$

$$y_1(0) = 0, y_2(0) = t, y_3(0) = 4CMa. \quad (44)$$

Introducing the shooting parameters t as $y_2(0) = t$, then the equations (43)-(44) are converted into the equations (45)-(46) as follow:

$$\begin{cases} (\frac{\partial y_1}{\partial t})' = \frac{\partial y_1'}{\partial t} = \frac{\partial y_2}{\partial t} \\ (\frac{\partial y_2}{\partial t})' = \frac{\partial y_2'}{\partial t} = \frac{\partial y_3}{\partial t} \\ (\frac{\partial y_3}{\partial t})' = \frac{\partial y_3'}{\partial t} = P\frac{\partial y_2}{\partial t} + A(y_3\frac{\partial y_1}{\partial t} + y_1\frac{\partial y_3}{\partial t} - y_2\frac{\partial y_2}{\partial t}) \end{cases}, \quad (45)$$

$$\frac{\partial y_1}{\partial t}|_{\xi=0} = 0, \frac{\partial y_2}{\partial t}|_{\xi=0} = 1, \frac{\partial y_3}{\partial t}|_{\xi=0} = 0. \quad (46)$$

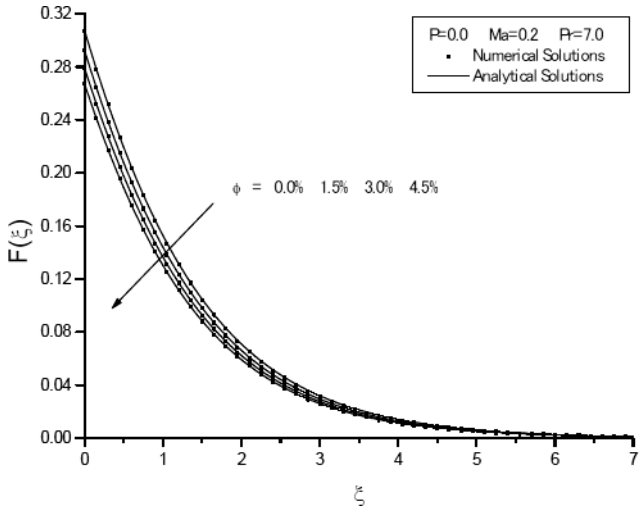

FIG. 4. Effects of the solid volume fraction on the velocity.

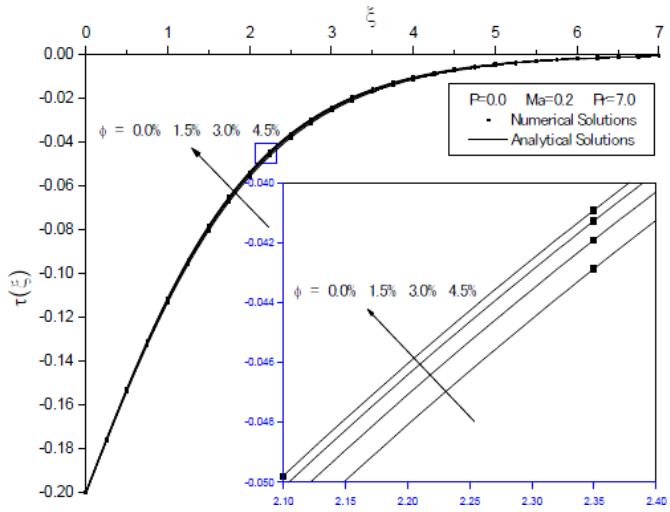

FIG. 5. Effects of the solid volume fraction on the shear stress.

We use the shooting method coupled with the Runge-Kutta scheme and the Newton method to solve the boundary value problem (15)-(16) with (18). The programming ideas as follows:

(1) Give initial values to the shooting parameter $y_2(0) = t_0$.
(2) Get the results of the equations (43)-(44) $\{{y_1}^0, {y_2}^0, {y_3}^0\}$ by the classical fourth-order Runge-Kutta scheme.
(3) Judge the iteration condition $|y_2(\infty) - 0| < \varepsilon$, where ε is the iteration accuracy. If the results of (2) meet the iteration conditions, $\{{y_1}^0, {y_2}^0, {y_3}^0\}$ is the solution of the equations (15)-(16) with (17). The iteration loop is over. Otherwise, the next step is executed.
(4) Use the Newton method to revise the shooting parameters as

$$t_{k+1} = t_k - \frac{y_2(t_k) - 0}{\partial y_2(t_k)/\partial t_k}. \tag{47}$$

Equations (45)-(46) are used to obtain the item $\partial y_2(t_k)/\partial t_k$ in the fixed equation (47). The steps (1)-(3) are re-executed until the new results of the step (2) meet the iteration conditions. In the same way, we can obtain the solutions for the equation (17) with condition (19), we omitted here.

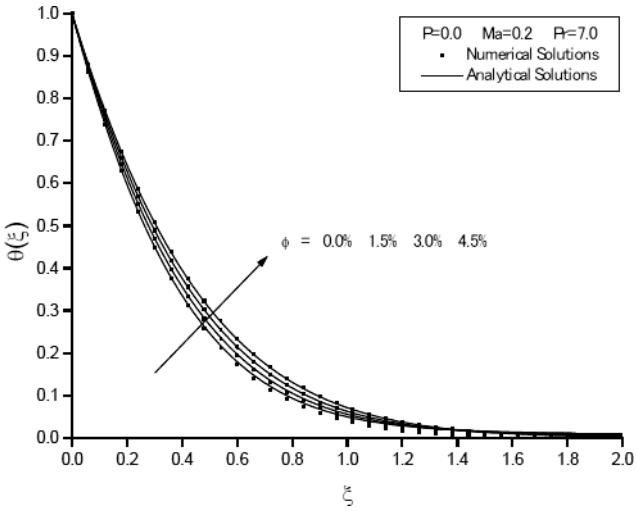

FIG. 6. Effects of the solid volume fraction on the temperature.

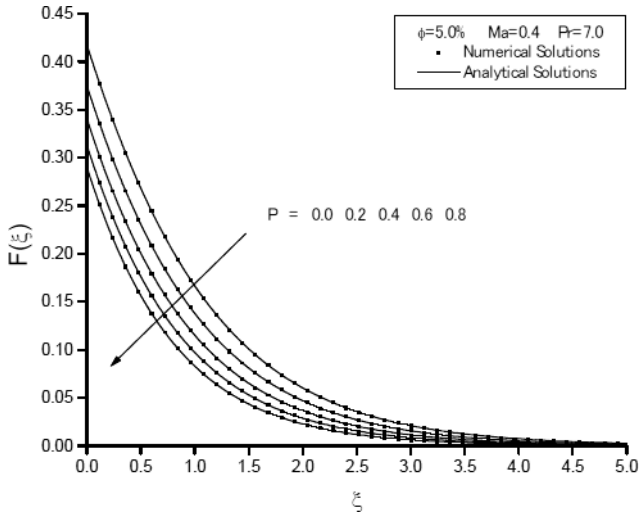

FIG. 7. Effects of the permeability parameter on the velocity.

VI. RESULTS AND DISCUSSION

In the section 'Homotopy analysis solutions', we get the solutions of $H(\xi)$ and $\theta(\xi)$ by the Homotopy analysis method (HAM). As pointed by Liao,[38] the convergence of these series strongly depends upon the value of the auxiliary parameters h_H and h_θ. In order to seek the admissible values of h_H and h_θ, we plot the h–curves at 10^{th}-order approximation of them in Figs. 2-3. Since the interval for the admissible values of h_H and h_θ correspond to the line segments nearly parallel to the horizontal axis, then we know that the admissible for the parameters h_H and h_θ are $-2.0 \le h_H \le -0.3$ and $-1.6 \le h_\theta \le -0.5$ when $\phi = 5.0\%$, $P = 0.0$, $Ma = 0.3$ and Pr = 7.0. In this situation, we choose $h = -1.0$ and get $H'(0) = -0.690188$ ($F(0) = -0.5H'(0) = 0.345094$) and $\theta'(0) = -2.35211$. In the section 'Numerical solutions', we get the solutions of $H(\xi)$ and $\theta(\xi)$ by the shooting method. Tables 2-4 present different values of $F(0)$, $H(\infty)$ and $\theta'(0)$ for different values of the solid volume fraction, the permeability parameter and the Marangoni parameter. From the comparison listed in Tables 2-4 we can see that the analytical solutions (HAM) agree well with the numerical solutions. Then the effects of the solid volume fraction, the permeability parameter and the Marangoni parameter on the velocity and temperature fields are analyzed and discussed in detail in this section.

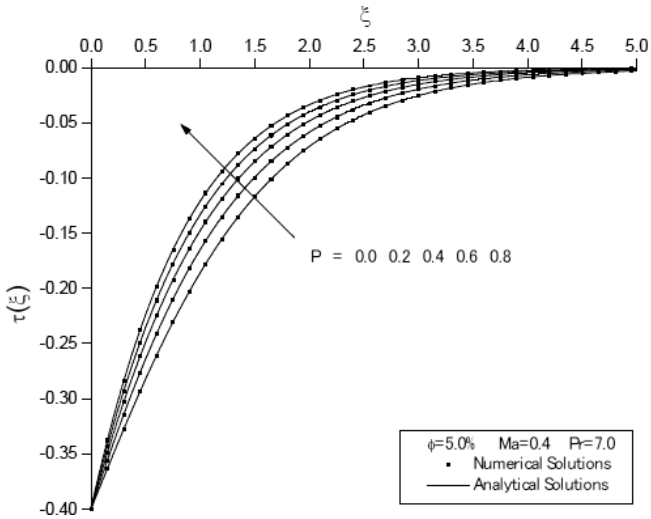

FIG. 8. Effects of the permeability parameter on the shear stress.

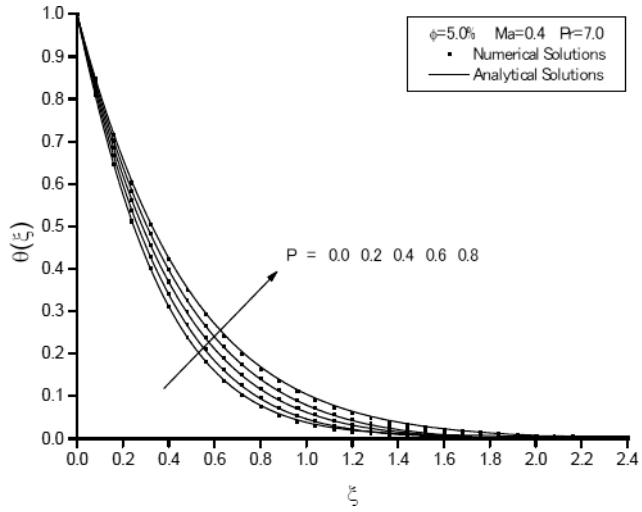

FIG. 9. Effects of the permeability parameter on the temperature.

Figs. 4-6 (Figs. 7-9) present effects of the solid volume fraction (the permeability parameter) on the velocity, the shear stress and the temperature. From these figures, we can see that the velocity, the shear stress and the temperature decrease and converged to zero as the location similarity variable increases. The values of the shear stress are non-positive and there has a same value of the dimensionless shear stress on the interface, i.e. $\tau(0) = -0.20$ when $P = 0.0$, $Ma = 0.2$, Pr = 7.0 for all the solid volume fraction $\phi = 0.0\%, 1.5\%, 3.0\%, 4.5\%$, and $\tau(0) = -0.40$ when $\phi = 4.5\%$, $Ma = 0.40$, Pr = 7.0 for all the permeability parameter $P = 0.0, 0.2, 0.4, 0.6, 0.8$. These trends all meet the features of the Marangoni boundary layer. The velocity and the shear stress decrease while the temperature increases as the solid volume fraction (the permeability parameter) increases. In other word, the velocity boundary layer thinner while the temperature boundary layer thicker as the solid volume fraction (the permeability parameter) increases. It should be noted that the influences of the permeability parameter on the velocity, the shear stress and the temperature are similar to the results of the solid volume fraction, while the effects of permeability parameter are more obvious. For example, the distribution profiles of the shear stress $\tau(\xi) \sim \xi$ are obviously different for different values of the permeability parameter in Fig. 5, while there is no obvious difference in the distribution profiles of the shear stress $\tau(\xi) \sim \xi$ for different values of the solid volume fraction in Fig.8.

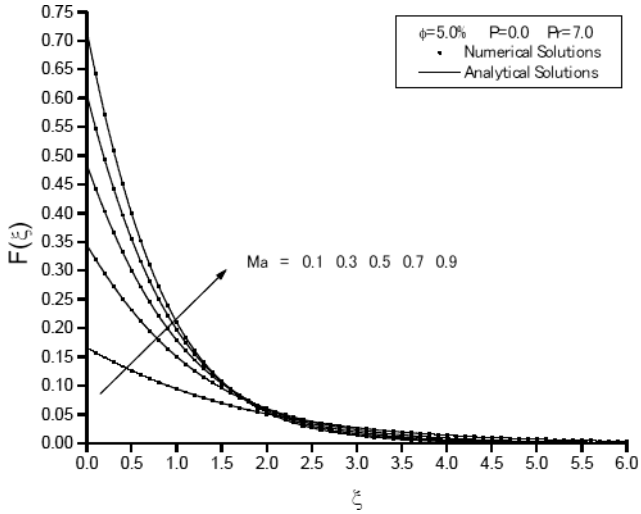

FIG. 10. Effects of the Marangoni parameter on the velocity.

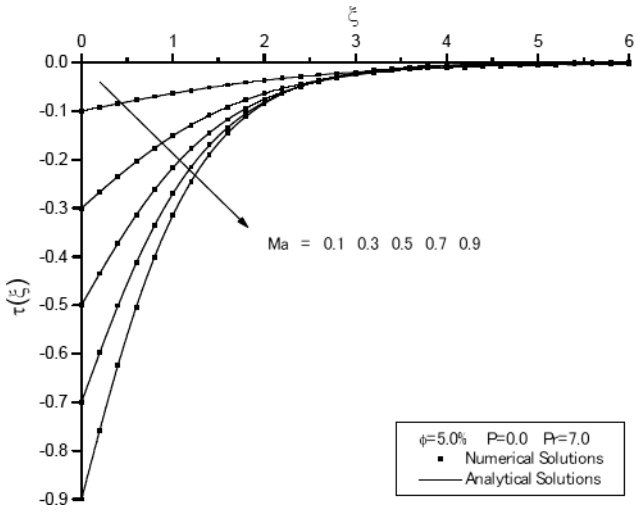

FIG. 11. Effects of the Marangoni parameter on the shear stress.

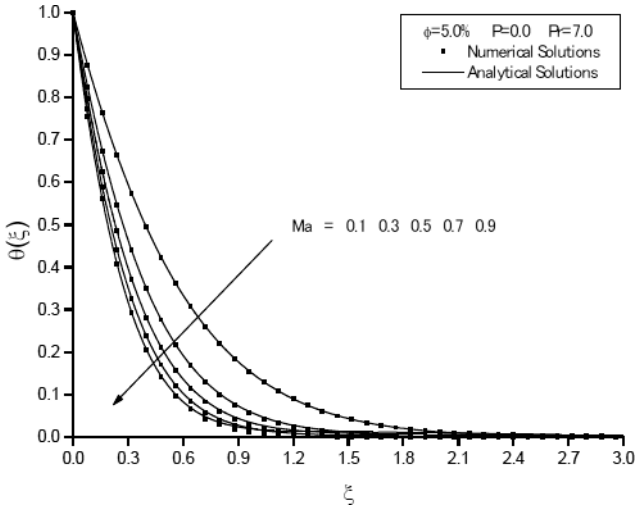

FIG. 12. Effects of the Marangoni parameter on the temperature.

Figs. 10-12 present effects of the Marangoni parameter on the velocity, the shear stress and the temperature. We observe from Figs. 10-11 that the velocity and the shear stress in the outer part of the velocity boundary layer decrease as the Marangoni parameter increases. Accordingly, the velocity boundary layer thickness increases with reducing values of the Marangoni parameter. It is interesting to see that the velocity profiles intersected each other in the near-surface region, where these intersections are found to occur at about $\xi \approx 1.5 - 2.5$ (the shear stress profiles: $\xi \approx 2.8 - 4.0$) when $\phi = 5.0\%$, $P = 0.0$ and $\mathrm{Pr} = 7.0$. It also can be seen that the temperature and the temperature boundary layer decrease as the Marangoni parameter increases.

VII. CONCLUSIONS

This paper presented an investigation for the Marangoni boundary layer flow and heat transfer of copper-water nanofluid over a porous medium disk. The governing partial differential equations were transformed into a two point boundary value problem using Kármán similarity transformation. The nonlinear ordinary differential equations subject to boundary conditions were solved by the Homotopy analysis method (HAM) and the shooting method coupled with Runge-Kutta scheme

and Newton method. It was found that the flow and heat transfer behaviors were strongly depending on the value of the solid volume fraction, the permeability parameter and the Maragoni parameter. The velocity, the shear stress and the velocity boundary layer decrease while the temperature increases as the solid volume fraction and the permeability parameter increase. The velocity (in the outer part), the shear stress (in the outer part), the temperature, the velocity boundary layer and the temperature boundary layer all decrease as the Marangoni parameter increases.

ACKNOWLEDGEMENTS

The research was supported by the Scientific Research Funds of Huaqiao University (No. 14BS310), the National Natural Science Foundations of China (Nos. 51276014 and 51476191).

APPENDIX

$$
\begin{aligned}
H_2(\xi) = \frac{1}{12}h^2CMa[&A^2C^2Ma^2\exp(-3\xi)\\
&+2ACMa(5P+6ACMa-3)\exp(-2\xi)+4ACMa(P+2ACMa-1)\xi\exp(-2\xi)\\
&+3(8P^2+30PACMa-8P+21A^2C^2Ma^2-16ACMa)\exp(-\xi)\\
&+(15P^2+64PACMa-18P+56A^2C^2Ma^2-40ACMa+3)\xi\exp(-\xi)\\
&+3(P^2+4PACMa-2P+4A^2C^2Ma^2-4ACMa+1)\xi^2\exp(-\xi)\\
&+2(-12P^2-45PACMa+12P-38A^2C^2Ma^2+27ACMa)],
\end{aligned}
$$

$$
\begin{aligned}
\theta_2(\xi) = \frac{1}{360}h^2[&-56BCMa(ACMa+28BCMa-2)\exp(-4\xi)\\
&+5(63PBCMa+98ABC^2Ma^2+1176B^2C^2Ma^2-343BCMa+12)\exp(-3\xi)\\
&-10(168PBCMa+252ABC^2Ma^2+784B^2C^2Ma^2-175BCMa+4)\exp(-2\xi)\\
&+(1365PBCMa+1946ABC^2Ma^2+3528B^2C^2Ma^2-1337BCMa-20)\exp(-\xi)],
\end{aligned}
$$

$$
\begin{aligned}
H_3(\xi) = \frac{h^3CMa}{216}[&5A^3C^3Ma^3\exp(-4\xi)+3A^2C^2Ma^2(24P+29ACMa+18ACMa\xi-12A)\exp(-3\xi)\\
&+9P^2ACMa(35+22\xi+4\xi^2)\exp(-2\xi)+144PA^2C^2Ma^2(6+5\xi+\xi^2)\exp(-2\xi)\\
&-18PACMa(15+14\xi+4\xi^2)\exp(-2\xi)+2A^3C^3Ma^3(289+288\xi+72\xi^2)\exp(-2\xi)\\
&-144A^2C^2Ma^2(3+3\xi+\xi^2)\exp(-2\xi)+9ACMa(3+6\xi+4\xi^2)\exp(-2\xi)\\
&+9P^3(48+33\xi+9\xi^2+\xi^3)\exp(-\xi)+18P^2ACMa(140+116\xi+31\xi^2+3\xi^3)\exp(-\xi)\\
&+27P^2(16+13\xi+5\xi^2+\xi^3)\exp(-\xi)+9PA^2C^2Ma^2(504+455\xi+128\xi^2+12\xi^3)\exp(-\xi)\\
&+36PACMa(60+52\xi+19\xi^2+3\xi^3)\exp(-\xi)+18ACMa(12+12\xi+7\xi^2+3\xi^3)\exp(-\xi)\\
&+27P(\xi+\xi^2+\xi^3)\exp(-\xi)+9A^2C^2Ma^2(252+231\xi+80\xi^2+12\xi^3)\exp(-\xi)\\
&+A^3C^3Ma^3(2585+2430\xi+720\xi^2+72\xi^3)\exp(-\xi)+9(3\xi+3\xi^2-\xi^3)\exp(-\xi)\\
&+(432P^2+2430PACMa+2736A^2C^2Ma^2-243ACMa)],
\end{aligned}
$$

$$
\begin{aligned}
\theta_3(\xi) = \frac{1}{43200}h^3[&-8064B^2C^2Ma^2(-2+ACMa+28BCMa)\exp(-6\xi)\\
&+140BCMa(-15A^2C^2Ma^2+9016B^2C^2Ma^2-2695BCMa+124)\exp(-5\xi)\\
&+140BC^2Ma^2(315PB+742A^2BCMa-32A)\exp(-5\xi)\\
&+224ABC^2Ma^2(61P+30P\xi+62ACMa+60A\xi)\exp(-4\xi)\\
&+1568AB^2C^3Ma^3(679+120\xi)\exp(-4\xi)-336ABC^2Ma^2(277+60\xi)\exp(-4\xi)\\
&+784B^2C^2Ma^2(799P+120P\xi-2039-120\xi)\exp(-4\xi)\\
&+56BCMa(2889+120\xi-829P-120P\xi)\exp(-4\xi)+160(17836B^3C^3Ma^3-27)\exp(-4\xi)\\
&+1575BCMa(39P^2+164PACMa+148A^2C^2Ma^2)\exp(-3\xi)\\
&+18900BCMa(P^2+4PACMa+4A^2C^2Ma^2)\xi\exp(-3\xi)
\end{aligned}
$$

$$-3150PBCMa(79+12\xi)\exp(-3\xi)-18900ABC^2Ma^2(23+4\xi)\exp(-3\xi)$$
$$+58800B^2C^2Ma^2(27P+42ACMa+56BCMa-43)\exp(-3\xi)$$
$$+75(3619BCMa+252BCMa\xi-32)\exp(-3\xi)$$
$$-16800BCMa(12P^2+45PACMa+38A^2C^2Ma^2)\exp(-2\xi)$$
$$-280BCMa(1155P+2258ACMa)\exp(-2\xi)-40(2737BCMa+20)\exp(-2\xi)$$
$$-3920B^2C^2Ma^2(435P+638ACMa+504BCMa-467)\exp(-2\xi)$$
$$+7BCMa(20025P^2+73052PACMa+60184A^2C^2Ma^2)\exp(-\xi)$$
$$+28B^2C^2Ma^2(24997P+35722ACMa+17864BCMa-19273)\exp(-\xi)$$
$$-2BCMa(8641P+20438ACMa)\exp(-\xi)-7(2503BCMa+160)\exp(-\xi)],$$

$\ldots,$

[1] Y.M. Xuan and W. Roetzel, "Conceptions of heat transfer correlation of nanofluids," International Journal Communications in Heat and Mass Transfer **43**, 3701-3707 (2000).
[2] R.A. Mahdi, H.A. Mohammed, K.M. Munisamy, and N.H. Saeid, "Review of convection heat transfer and fluid flow in porous media with nanofluid," Renewable and Sustainable Energy Reviews **41**, 715-734 (2015).
[3] M.A.A. Hamad, I. Pop, and A.I.M. Ismail, "Magnetic field effects on free convection flow of a nanofluid past a vertical semi-infinite flat plate," Nonlinear Analysis: Real World Applications **12**, 1338-1346 (2011).
[4] S. Ahmad and I. Pop, "Mixed convection boundary layer flow from a vertical flat plate embedded in a porous medium filled with nanofluids," International Communications in Heat and Mass Transfer **37**, 987-991 (2010).
[5] A.V. Rosca, N.C. Rosca, T. Grosan, and I. Pop, "Non-Darcy mixed convection from a horizontal plate embedded in a nanofluid saturated porous media," International Communications in Heat and Mass Transfer **39**, 1080-1085 (2012).
[6] Z.H. Khan, W.A. Khan, and I. Pop, "Triple diffusive free convection along a horizontal plate in porous media saturated by a nanofluid with convective boundary condition," International Journal of Heat and Mass Transfer **66**, 603-612 (2013).
[7] L. Tham, R. Nazar, and I. Pop, "Mixed convection flow from a horizontal circular cylinder embedded in a porous medium filled by a nanofluid: Buongiorno - Darcy model," International Journal of Thermal Sciences **84**, 21-33 (2014).
[8] F.M. Hady, F.S. Ibrahim, S.M. Abdel-Gaied, and M.R. Eid, "Effect of heat generation/absorption on natural convective boundary-layer flow from a vertical cone embedded in a porous medium filled with a non-Newtonian nanofluid," International Communications in Heat and Mass Transfer **38**, 1414-1420 (2011).
[9] A.M. Rashad, A.J. Chamkha, and M. Modather, "Mixed convection boundary-layer flow past a horizontal circular cylinder embedded in a porous medium filled with a nanofluid under convective boundary condition," Computers & Fluids **86**, 380-388 (2013).
[10] L.C. Zheng, C.L. Zhang, X.X. Zhang, and J.H. Zhang, "Flow and radiation heat transfer of a nanofluid over a stretching sheet with velocity slip and temperature jump in porous medium," Journal of the Franklin Institute **350**, 990-1007 (2013).
[11] F.M. Abbasi, T. Hayat, and B. Ahmad, "Peristaltic transport of copper-water nanofluid saturating porous medium," Physica E **67**, 47-53 (2015).
[12] K. Arafune and A. Hirata, "Thermal and solutal Marangoni convection in In-Ga-Sb system," Journal of Crystal Growth **197**, 811-817 (1999).
[13] A.M. Cazabat, F. Heslot, S.M. Troian, and P. Carles, "Fingering instability of thin spreading films driven by temperature gradients," Nature **346**, 824-826 (1990).
[14] D.M. Christopher and B.X. Wang, "Similarity simulation for Marangoni convection around a vapor bubble during nucleation and growth," International Journal of Heat and Mass Transfer **44**, 799-810 (2001).
[15] D.M. Christopher and B.X. Wang, "Prandtl number effects for Marangoni convection over a flat surface," International Journal of Thermal Sciences **40**, 564-570 (2001).
[16] J.R.A. Pearson, "On convection cells induced by surface tension," Journal of Fluid Mechanics **4**(5), 489-500 (1958).
[17] G.A. Mcconaghy and B.A. Finlayson, "Surface tension driven oscillatory instability in a rotating fluid layer," Journal of Fluid Mechanics **39**, 49-55 (1969).
[18] M. Bestehorn, A. Pototsky, and U. Thiele, "3D large scale Marangoni convection in liquid films," The European Physical Journal B **33**, 457-467 (2003).
[19] U. Thiele and E. Knobloch, "Thin liquid films on a slightly inclined heated plate," Physica D **190**, 213-248 (2004).
[20] L.C. Zheng, X.X. Zhang, and Y.T. Gao, "Analytical solution for Marangoni convection over a liquid-vapor surface due to an imposed temperature gradient," Mathematical and Computer Modelling **48**, 1787-1795 (2008).
[21] A.A. Mudhaf and A.J. Chamkha, "Similarity solutions for MHD thermosolutal Marangoni convection over a flat surface in the presence of heat generation or absorption effects," Heat and Mass Transfer **42**, 112-121 (2005).
[22] E. Magyari and A.J. Chamkha, "Exact analytical solutions for thermosolutal Marangoni convection in the presence of heat and mass generation or consumption," Heat and Mass Transfer **43**, 965-974 (2007).
[23] E. Magyari and A.J. Chamkha, "Exact analytical results for the thermosolutal MHD Marangoni boundary layers," International Journal of Thermal Sciences **47**, 848-857 (2008).
[24] Y. Zhang and L.C. Zheng, "Analysis of MHD thermosolutal Marangoni convection with the heat generation and a first-order chemical reaction," Chemical Engineering Science **69**, 449-455 (2012).
[25] Y. Zhang and L.C. Zheng, "Similarity solutions of Marangoni convection boundary layer flow with gravity and external pressure," Chinese Journal of Chemical Engineering **22**(4), 365-369 (2014).
[26] C.H. Chen, "Marangoni effects on forced convection of power-law liquids in a film over a stretching surface," Physics Letters A **370**, 51-57 (2007).

[27] S. Saravanan and T. Sivakumar, "Exact solution of Marangoni convection in a binary fluid with throughflow and Soret effect," Applied Mathematical Modelling **33**, 3674-3681 (2009).
[28] M. Saleem, M.A. Hossain, S. Mahmud, and I. Pop, "Entropy generation in Marangoni convection flow of heated fluid in an open ended cavity," International Journal of Heat and Mass Transfer **54**, 4473-4484 (2011).
[29] L.C. Zheng, Y.H. Lin, and X.X. Zhang, "Marangoni convection of power law fluids driven by power-law temperature gradients," Journal of the Franklin Institute **349**, 2585-2597 (2012).
[30] Y.H. Lin, L.C. Zheng, and X.X. Zhang, "Magnetohydrodynamics thermocapillary Marangoni convection heat transfer of power-law fluids driven by temperature gradient," Journal of Heat Transfer **135**, 051702-6 (2013).
[31] Y.H. Lin, L.C. Zheng, and X.X. Zhang, "Radiation effects on Marangoni convection flow and heat transfer in pseudo-plastic non-Newtonian nanofluids with variable thermal conductivity," International Journal of Heat and Mass Transfer **77**, 708-716 (2014).
[32] A. Mahdy and S.E. Ahmed, "Thermosolutal Marangoni boundary layer magnetohydrodynamic flow with the Soret and Dufour effects past a vertical flat plate," Engineering Science and Technology, an International Journal **18**, 24-31 (2015).
[33] C.R. Jiao, L.C. Zheng, and L.X. Ma, "MHD thermosolutal marangoni convection heat and mass transport of power law fluid driven by temperature and concentration gradient," AIP Advances **5**, 087160 (2015).
[34] T. Hayat, U. Shaheen, A. Shafiq, A. Alsaedi, and S. Asghar, "Marangoni mixed convection flow with Joule heating and nonlinear radiation," AIP Advances **5**, 077140 (2015).
[35] C.Y. Ming, L.C. Zheng, and X.X. Zhang, "Steady flow and heat transfer of the power-law fluid over a rotating disk," International Communications in Heat and Mass Transfer **38**, 280-284 (2011).
[36] N. Bachok, A. Ishak, and I. Pop, "Flow and heat transfer over a rotating porous disk in a nanofluid," Physica B **406**, 1767-1772 (2011).
[37] H.C. Brinkman, "The viscosity of concentrated suspensions and solutions," The Journal of Chemical Physics **20**, 571-571 (1952).
[38] S.J. Liao, *Beyond Perturbation: Introduction to the Homotopy Analysis Method* (Chapman & Hall/, CRC Press, Baca Raton, 2003).
[39] S.J. Liao, *Homotopy Analysis Method in Nonlinear Differential Equations* (Springer, Berlin, 2012).